Environmental Science and Engineering

Sijing Wang
Runqiu Huang
Rafig Azzam
Vassilis P. Marinos *Editors*

Engineering Geology for a Habitable Earth: IAEG XIV Congress 2023 Proceedings, Chengdu, China

Volume 4: Technological Innovation and Application for Engineering Geology

Springer

Environmental Science and Engineering

Series Editors

Ulrich Förstner, Buchholz, Germany

Wim H. Rulkens, Department of Environmental Technology, Wageningen, The Netherlands

The ultimate goal of this series is to contribute to the protection of our environment, which calls for both profound research and the ongoing development of solutions and measurements by experts in the field. Accordingly, the series promotes not only a deeper understanding of environmental processes and the evaluation of management strategies, but also design and technology aimed at improving environmental quality. Books focusing on the former are published in the subseries Environmental Science, those focusing on the latter in the subseries Environmental Engineering.

Sijing Wang · Runqiu Huang · Rafig Azzam ·
Vassilis P. Marinos
Editors

Engineering Geology for a Habitable Earth: IAEG XIV Congress 2023 Proceedings, Chengdu, China

Volume 4: Technological Innovation and Application for Engineering Geology

Springer

Editors
Sijing Wang
Department of Hydraulic Engineering
Tsinghua University
Beijing, China

Rafig Azzam
Department of Engineering Geology
and Hydrogeology
RWTH Aachen University
Aachen, Germany

Runqiu Huang
Chengdu University of Technology
Chengdu, Sichuan, China

Vassilis P. Marinos
School of Civil Engineering
National Technical University of Athens
Zografou, Greece

ISSN 1863-5520 ISSN 1863-5539 (electronic)
Environmental Science and Engineering
ISBN 978-981-99-9068-9 ISBN 978-981-99-9069-6 (eBook)
https://doi.org/10.1007/978-981-99-9069-6

This Springer imprint is published by the registered company Springer Nature Singapore Pte Ltd.
The registered company address is: 152 Beach Road, #21-01/04 Gateway East, Singapore 189721, Singapore

Academic Committee

Academic Committee Chairs

Sijing Wang
Runqiu Huang

Academic Committee Members

Anthony Bowden
Bin Shi
Bo An-Jang
Carlos Delgado
Charles W. W. Ng
Chungsik Yoo
Defang Kong
Dingcheng Huang
Faquan Wu
Fawu Wang
Helen Reeves
Hengxing Lan
Hsein Juang
Huiming Tang
Janusz Wasowski
Jean Hutchinson
Jean-Alain Fleurisson
Jian Yang
Jianbing Peng
Jianmin Zhang
Jianxin Hua

Jinxiu Yan
John Ludden
Julien Cohen-Waeber
Kyoji Sassa
Lansheng Wang
Manchao He
Martin Culshaw
Moshood Niyi Tijani
Nicola Casagli
Niek Rengers
Peng Cui
Qing Wang
Rafig Azzam
Ranjan Kumar Dahal
Resat Ulusay
Ricardo Oliveira
Roger Frank
Scott F. Burns
Shitian Wang
Shutao Yang
Vassilis Marinos
Victor Manuel Hernandez Madrigal
Wei Wu
Wei Zhang
Xiao Li
Xiating Feng
Yong-Seok Seo
Yueping Yin
Yusheng Gao
Zelian Chen
Zuyu Chen

Organizing Committee Chairs

Qiang Xu
Qiangbing Huang
Shengwen Qi
Xiangjun Pei
Xiaoqing Chen
Yuyong Jiao
Xuanmei Fan

Organizing Committee Members

Chaojun Ouyang
Chaosheng Tang
Jianjun Zhao
Liangqing Wang
Ning Liang
Wen Zhang
Yuhuan Song

Preface

The XIV Congress of the International Association for Engineering Geology and the Environment (XIV IAEG Congress 2023) was successfully held in Chengdu, China from September 21 to 27, 2023. Focusing on the main theme "Engineering Geology for a Habitable Earth", researchers and practitioners worldwide from academia, industry, and government have joined us in this prestigious event. Based on the topics discussed at the congress, the proceedings are organized into six volumes as follows:

- Volume 1: Engineering Geomechanics of Rock and Soil Masses
- Volume 2: Geohazard Mechanisms, Risk Assessment and Control, Monitoring and Early Warning
- Volume 3: Active Tectonics, Geomorphology, Climate and Geoenvironmental Engineering Geology
- Volume 4: Technological Innovation and Applied for Engineering Geology
- Volume 5: Megacity Development and Preservation of Cultural Heritage Engineering Geology
- Volume 6: Marine and Deep Earth Engineering Geology

Meanwhile, on behalf of the organizing committee, we would also like to express our deepest appreciation to the technical program committee members, reviewers, session chairs, and volunteers for their strong support for congress.

Last but not the least, our gratitude also goes to the editors and press for their great support to the congress.

September 2023 XIV IAEG Congress 2023 Organizing Committee

Contents

Chapter 1
On Stability of a Slope with Bedrock Using the Upper Bound Limit Analysis

Bing Yang, Jiangrong Hou, Xushen Zheng, Guoyi Wang, Songke Song, and Yang Luo

Abstract The potential failure modes and stability of a slope with bedrock was investigated systematically based on the upper bound limit analysis in this paper. The effect of interface between bedrock and soil on the slope stability was discussed in detail. The equations for calculating safety factors for three possible failure modes of the slope with bedrock due to gravity were derived. The most dangerous failure mode of the slope was determined using a program to optimize the solution to the stability equation for the slope. Finally, the effects of the inclination angle along the interface, the controlling angle of the interface position, the slope angle, and the interface strength parameters on the failure mode and safety factor were examined quantitatively. The results show that the relative position of the bedrock-soil interface and the empty surface of the slope is an important factor affecting the stability of the slope. Regarding to global failure along the interface between bedrock and soil (Mode 1 in this paper), the safety factor decreases at first and then increases as the inclination angle at the upper part of the interface increases. The shear strength parameters along the interface have a significant influence on the failure mode and safety factor.

B. Yang · J. Hou · X. Zheng · Y. Luo
School of Civil Engineering, Southwest Jiaotong University, Chengdu 610031, People's Republic of China
e-mail: yangb@home.swjtu.edu.cn

J. Hou
e-mail: jiangronghou@my.swjtu.edu.cn

J. Hou
South China Institute of Geotechnical Engineering, South China University of Technology, Guangzhou 510641, Guangdong, China

G. Wang
CLP Construction Investment Co., Ltd, Chengdu 610212, People's Republic of China

S. Song (✉)
Sichuan Transportation Survey and Design Institute Co., Chengdu 610017, People's Republic of China
e-mail: 54881770@qq.com

S. Wang et al. (eds.), *Engineering Geology for a Habitable Earth: IAEG XIV Congress 2023 Proceedings, Chengdu, China*, Environmental Science and Engineering,
https://doi.org/10.1007/978-981-99-9069-6_1

Keywords Slope with bedrock · Limit analysis · Slope stability · Failure mode · Safety factor

1.1 Introduction

The analysis of slope stability has received wide attention for decades due to its practical importance (Fellenius 1927; Bishop 1955; Janbu 1973; Morgenstern and Price 1965; Spencer 1967; Duncan and Wright 1980; Chen and Morgenstern 1983; Zhu and Lee 2002; Griffiths and Marquez 2007). The application of limit analysis to earth slopes was started by Drucker and Prager (1952), who applied the kinematic approach of limit analysis to the stability of slopes undergoing plane-strain failure. Both translational and rotational failure mechanisms were considered in their study. The limit analysis based on the log-spiral mechanism for simple slopes was proposed by Chen et al. (1969). A variety of solutions to a wide range of problems using this method can be found in the monograph by Chen (1975). At the same time, the upper bound analysis was used by some researchers (Karal 1977a, b; Chen and Chan 1984; Izbicki 1981). Extensions of the upper bound solutions to nonlinear failure envelopes have been investigated by Baker and Frydman (1983), Zhang and Chen (1987), Drescher and Christopoulos (1988), and Collins et al. (1988). Later, Donald and Chen (1997) systematically elaborated the theoretical background, numerical techniques, validations and extensions of a new upper bound slope stability analysis method. Moreover, the influence of pore water pressure, seismic effects, and soil reinforcement were investigated by Michalowski (1995, 1998, 1999). Major contributions for soil slope stability analysis were presented by Michalowski and his co-worker who provided sets of stability charts for cohesive-frictional slopes which took seismic loadings and pore pressure into account (Michalowski 2002; Viratjandr and Michalowski 2006). Through using both lower and upper bound analyses to estimate slope stability, several researchers proposed sets of stability charts for inhomogeneous soil slopes and cohesive-frictional soil slopes subjected to pore pressure and seismic loadings respectively (Yu et al. 1998; Kim et al. 1999; Loukidis et al. 2003).

The stability of an inhomogeneous slope has been also investigated by many researchers (Rulon and Freeze 1985; Cho 2007; Damiano and Olivares 2010; Lianheng et al. 2013; Zhan et al. 2013; Liu et al. 2015; Tingkai et al. 2016). Lianheng et al. (2013) analyzed the stability of slopes reinforced with prestressed anchor cables based on upper bound limit analysis. Tingkai et al. (2016) investigated the stability of a slope that was reinforced with a row of piles using limit analysis method.

Slopes with bedrock are a kind of slopes whose lower parts are bedrock and the upper parts are a loose accumulation body, and the sliding mass are located within the upper parts, namely, the overburden layer. However, the failure modes may be different in this type of slopes and those homogeneous slopes. The influence of the bedrock-soil interface on the failure mode and safety factor may not be ignored. At present, little studies have systematically investigated the effects of interface between bedrock and soil on the stability of slopes, although many studies may involve this type of slope. When the bedrock exists in a slope, the slip surface determined by the traditional rotational failure mechanism may pass through the bedrock layer. Obviously, this does not correspond to an actual situation and will decrease the safety factor of the slope. Therefore, the position of the critical slip surface in an actual slope should be moved up.

In this paper, a new method based on upper bound limit analysis is given to investigate the stability of slopes with bedrock. The constraint conditions for the presence of bedrock were introduced into the equations for calculating safety factors of slopes using the upper bound limit analysis. The most dangerous failure mode of the slope will be examined. Furthermore, the effects of the inclination angle along the interface, the controlling angle of the interface position, the slope angle, and the interface strength parameters on the failure mode and safety factor will be investigated.

1.2 The Method for Predicting Stability of a Slope with Bedrock

The slope model considered in this study is shown in Fig. 1.1. Line BCD is the interface between bedrock and the overburden layer, which is assumed that it can generalize the shape of interfaces of most slopes. According to our previous work shows that mainly three kinds of failure modes may arise (Yang 2019). Although the three failure modes cannot cover all the cases, it nearly involves most of the cases. Therefore, only three failure modes have been considered in this paper. The first is global failure along the interface between bedrock and the overburden layer, which is defined as Mode 1. The second is local failure of the log-spiral slip surface due to cracking at the top of the slope, which is defined as Mode 2. The third is local failure of the slope with a log-spiral slip surface due to cracking in the slope (Mode 3). The three failure modes are shown in Fig. 1.1. The equations for calculating the safety factor of the slope for each mode will be derived.

1.2.1 Failure in Mode 1

The global failure mechanism of the slope is shown in Fig. 1.2, where BCD is the interface between bedrock and the overburden layer, i.e., the slip surface. The soil is divided into two portions by the vertical velocity discontinuity surface (CE) of the turning point (C) over the sliding surface. Each portion was treated as a rigid body, and the slip surface (BCD) and velocity discontinuity surface (CE) between the two portions were treated as a plastic body that dissipates energy.

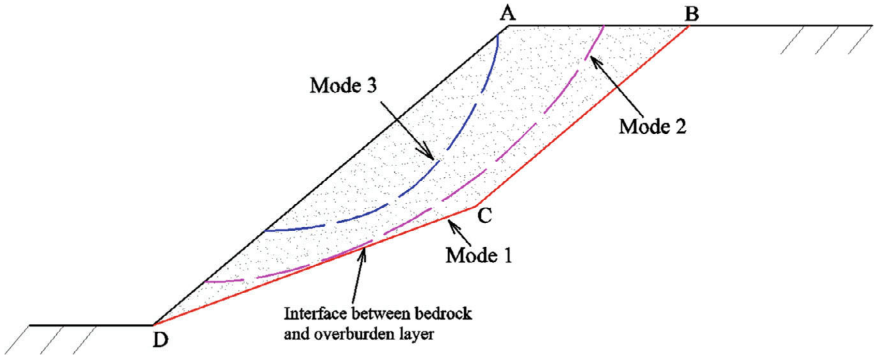

Fig. 1.1 Schematic diagram of the three failure modes

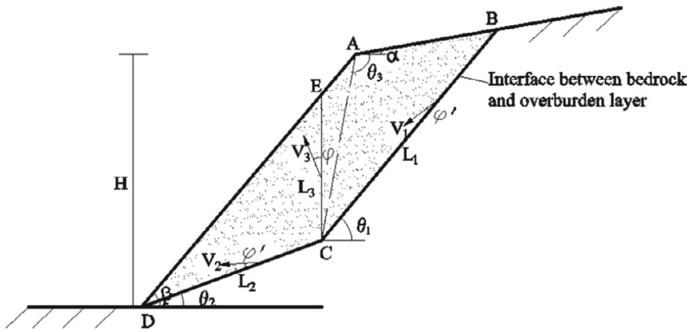

Fig. 1.2 Schematic showing the global failure mode (Mode 1)

The geometric parameters of slope shown in Fig. 1.2 are defined as follows: H is the slope height, γ is the unit weight of the soil, β is the slope angle, α is the slope inclination, θ_3 is the angle between AC and the horizontal line, θ_1 is the dip angle of the slip surface BC, L_1 is the length of BC, θ_2 is the dip angle of slip surface CD, L_2 is the length of CD, and L_3 is the length of the discontinuity surface CE. θ_3 will influence the position and length of lines BC and CD. The internal friction angle and soil cohesion in slope are φ and c, respectively. The equivalent internal friction angle and soil cohesion at the interface between bedrock and the overburden layer are φ' and c'. Suppose that the velocities at the slip surface BC and CD are V_1 and V_2, respectively. The relative velocity at discontinuity surface CE is V_3. . According to the associated flow rule, the angle between the velocities at the sliding surface (V_1 and V_2) and the sliding surface is φ', and the angle between V_3 and the discontinuity surface (CE) is φ.

According to geometric relationships among V_1, V_2, and V_3 in Fig. 1.2, the following equations hold:

$$V_2 = \frac{\cos\left(\theta_1 - \varphi - \varphi'\right)}{\cos(\varphi + \varphi' - \theta_2)} V_1 \tag{1.1}$$

$$V_3 = \frac{\sin(\theta_1 - \theta_2)}{\cos(\theta_2 - \varphi - \varphi')} V_1 \tag{1.2}$$

The strength reduction technique was introduced in the upper bound of limit analysis method in order to obtain the safety factor of the slope (Donald and Chen 1997; Michalowski 1998). The reduced shear strength parameters can be expressed as

$$\left.\begin{aligned} c_m &= \tfrac{c}{F} \\ \tan\varphi_m &= \tfrac{\tan\varphi}{F} \end{aligned}\right\} \tag{1.3}$$

$$\left.\begin{aligned} c'_m &= \tfrac{c'}{F} \\ \tan\varphi'_m &= \tfrac{\tan\varphi'}{F} \end{aligned}\right\} \tag{1.4}$$

where F is the strength reduction factor.

Rate of External Work. In this study, the only external load acting on slope only considers gravity. Then the work done by the external force only includes that by gravity. The corresponding rate of external work can be expressed as

$$W_{ext} = W_{G_1} + W_{G_2} = \gamma S_1 V_1 \sin\left(\theta_1 - \varphi'_m\right) + \gamma S_2 V_2 \sin\left(\theta_2 - \varphi'_m\right) \tag{1.5}$$

where S_1 and S_2 are the volume per unit width of the two portions of the soil, respectively. When $\theta_3 \geq 90°$,

$$S_1 = \left\{ \frac{\sin(\theta_1 + \theta_3)[\sin\theta_3 \sin(\theta_1 - \alpha) + \sin\alpha \sin(\theta_1 + \theta_3)]}{2\sin\theta_1 \sin(\theta_1 - \alpha)} - \frac{\cos\theta_3 \sin(\beta + \theta_3)}{2\cos\beta} \right\} \cdot f_1^2 H^2 \tag{1.6}$$

$$S_2 = \frac{\sin(\beta + \theta_3)(\cos\beta + \sin\beta\cos\theta_3 \cdot f_1)}{\sin(2\beta)} f_1 H^2 \tag{1.7}$$

In contrast, when $\theta_3 < 90°$,

$$S_1 = \left\{ \frac{\sin(\theta_1 + \theta_3)[\sin\theta_3 \sin(\theta_1 - \alpha) + \sin\alpha \sin(\theta_1 + \theta_3)]}{2\sin\theta_1 \sin(\theta_1 - \alpha)} - \frac{\cos\theta_3 \sin(\alpha + \theta_3)}{2\cos\alpha} \right\} \cdot f_1^2 H^2 \tag{1.8}$$

$$S_2 = \left[\frac{\sin(\beta+\theta_3)}{2\sin\beta} + \frac{\cos\theta_3\sin(\theta_3+\alpha)\cdot f_1}{2\cos\alpha}\right]\cdot f_1 H^2 \tag{1.9}$$

where $f_1 = \frac{\sin(\beta-\theta_2)}{\sin\beta\sin(\theta_2+\theta_3)}$.

Rate of Internal Energy Dissipation. Three processes contribute to the rate of internal energy dissipation: the rate of dissipation of energy along interface BC and CD ($\boldsymbol{W}_1$ and $\boldsymbol{W}_2$, respectively) and that along the velocity discontinuity surface CE ($\boldsymbol{W}_3$).

The total rate of energy dissipated is

$$W_{int} = W_1 + W_2 + W_3 \tag{1.10}$$

where

$$W_1 = c'_m V_1 \cos\varphi'_m L_1 = c'_m H V_1 f_1 \cos\varphi'_m \frac{\sin(\theta_3+\alpha)}{\sin(\theta_1-\alpha)} \tag{1.11}$$

$$W_2 = c'_m V_2 \cos\varphi'_m L_2 = c'_m H V_2 f_1 \cos\varphi'_m \frac{\sin(\beta+\theta_3)}{\sin(\beta-\theta_2)} \tag{1.12}$$

When $\theta_3 \geq 90°$,

$$W_3 = c_m V_3 \cos\varphi_m L_3 = c_m H V_3 f_1 \cos\varphi_m \frac{\sin(\beta+\theta_3)}{\cos\beta} \tag{1.13}$$

In contrast, when $\theta_3 < 90°$,

$$W_3 = c_m V_3 \cos\varphi_m L_3 = c_m H V_3 f_1 \cos\varphi_m \frac{\sin(\alpha+\theta_3)}{\cos\alpha} \tag{1.14}$$

Determination of Safety Factor. According to the upper limit theorem of limit analysis, let the rate of external work be equal to the rate of internal energy dissipation, i.e.,

$$W_{ext} = W_{int} \tag{1.15}$$

The critical height of the slope (H_{cr}) can be obtained from Eqs. (1.1)–(1.15):

$$H_{cr} = \frac{1}{\gamma} f\left(\theta_1, \theta_2, \theta_3, \beta, \alpha, c, \varphi, c', \varphi', F\right) \tag{1.16}$$

According to the optimization method proposed by Chen (1992), which was used to solve Eq. (1.16), and the minimum safety factor can be determined.

1.2.2 Failure in Mode 2

Figure 1.3 shows a diagram of local failure of the log-spiral slip surface due to cracking at the top of the slope. The log-spiral slip surface is GI, which can be expressed as

$$r = r_0 e^{[(\theta-\theta_0)\tan\varphi_m]} \tag{1.17}$$

where r_0 is the length of OG, θ_0 is the angle between OG and the positive x direction. r_h is the length of OI and θ_h is the angle between OI and the positive x direction. θ' and θ' are the inclination angles of OF and OF′. L is the crack length at the top of the slope (i.e., AG). β is the slope angle, α is the inclination angle at the top of the slope, H' is the height of the sliding body, H is the slope height, and l_1 is the length of DI on the slope.

Work-energy Balance Equation. The logarithmic-spiral failure mechanism of the slope shown in Fig. 1.3 is determined by the rate of external work due to gravity:

$$W_{ext} = \gamma r_0^3 \Omega (f_1 - f_2 - f_3) \tag{1.18}$$

where γ is specific weight of the soil, Ω is the rotational angular velocity, and f_1, f_2, and f_3 are defined in Eqs. (1.21)–(1.23). The rate of internal energy dissipation along the velocity discontinuity surface (GI) is as follows:

$$W_{int} = \int_{\theta_0}^{\theta_h} c_m (V\cos\varphi_m)\frac{rd\theta}{\cos\varphi_m} = \frac{c_m r_0^2 \Omega}{2\tan\varphi_m}\{\exp[2(\theta_h-\theta_0)\tan\varphi_m] - 1\} \tag{1.19}$$

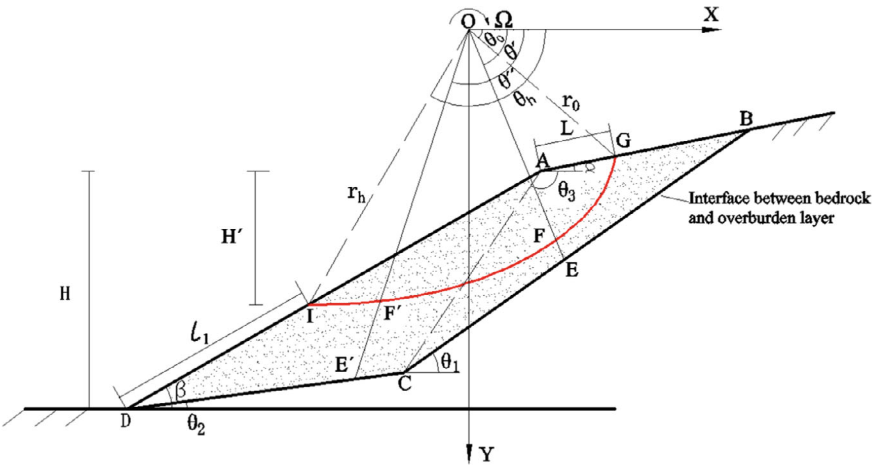

Fig. 1.3 Schematic showing the failure in Mode 2

If $W_{ext} = W_{int}$, then

$$\gamma r_0(f_1 - f_2 - f_3) = \frac{c_m}{2\tan\varphi_m}\{\exp[2(\theta_h - \theta_0)\tan\varphi_m] - 1\} \tag{1.20}$$

Where

$$f_1 = \{(3\tan\varphi_m \cos\theta_h + \sin\theta_h)\exp[3(\theta_h - \theta_0)\tan\varphi_m] - 3\tan\varphi_m\cos\theta_0 \\ - \sin\theta_0\}/3\left(1 + 9\tan^2\varphi_m\right) \tag{1.21}$$

$$f_2 = \frac{1}{6}\frac{L}{r_0}(2\cos\theta_0 - \frac{L}{r_0}\cos\alpha)\sin(\theta_0 + \alpha) \tag{1.22}$$

$$f_3 = \frac{1}{6}\exp[(\theta_h - \theta_0)\tan\varphi_m][\sin(\theta_h - \theta_0) - \frac{L}{r_0}\sin(\theta_h + \alpha)] \\ \cdot \{\cos\theta_0 - \frac{L}{r_0}\cos\alpha + \cos\theta_h\exp[(\theta_h - \theta_0)\tan\varphi_m] \tag{1.23}$$

$$r_0 = \frac{\sin(\beta - \alpha)(H - l_1\sin\beta)}{\sin\beta\{\sin(\theta_h + \alpha)\exp[(\theta_h - \theta_0)\tan\varphi_m] - \sin(\theta_0 + \alpha)\}} \tag{1.24}$$

$$\frac{L}{r_0} = \frac{\sin(\theta_h - \theta_0)}{\sin(\theta_h + \alpha)} - \frac{\sin(\theta_h + \beta)}{\sin(\theta_h + \alpha)\sin(\beta - \alpha)} \\ \{\sin(\theta_h + \alpha)\exp[(\theta_h - \theta_0)\tan\varphi_m] - \sin(\theta_0 + \alpha)\} \tag{1.25}$$

Suppose that the slope of a point F on the curve GI is the same as the slope of the straight line BC. Suppose further that OF is extended and intersects with the straight line BC at point E. Similarly, assume that the slope of point F′ is the same as the slope of CD. Suppose further that OF′ is extended and intersects with CD at point E′.

In order to ensure that the logarithmic spiral curve GI is above the interface BCD, it is necessary to include constraint conditions when calculating the homogeneous slope stability.

According to the relationship between polar and Cartesian coordinates, the slope at any point on the logarithmic spiral GI in Cartesian coordinates can be expressed as

$$k = \frac{\tan\varphi_m\sin\theta + \cos\theta}{\tan\varphi_m\cos\theta - \sin\theta}(0 < \theta < \pi) \tag{1.26}$$

It is also easy to show that the slope of the line BC is

$$k_1 = -\tan\theta_1 \tag{1.27}$$

When k = k1, then $\theta = \theta'$, i.e.,

$$\frac{\tan\varphi_m \sin\theta' + \cos\theta'}{\tan\varphi_m \cos\theta' - \sin\theta'} + \tan\theta_1 = 0(0 < \theta' < \pi) \tag{1.28}$$

The equation of the line OE is

$$\mathrm{y} = \tan\theta' x \tag{1.29}$$

According to the geometric relationship, the coordinates of D point are

$$\begin{cases} x_D = r_h\cos\theta_h - l_1\cos\beta \\ y_D = r_h\sin\theta_h + l_1\sin\beta \end{cases} \tag{1.30}$$

where $\mathrm{r_h} = \mathrm{r_0} \exp[(\theta_\mathrm{h} - \theta_0)\tan\varphi_\mathrm{m}]$.

In the triangle ACD, the length of line CD can be expressed as

$$|\mathrm{CD}| = \frac{\sin(\beta + \theta_3)}{\sin\beta\sin(\theta_2 + \theta_3)} H \tag{1.31}$$

According to the geometric relationship, the coordinates of point C are

$$\begin{cases} x_C = x_D + |\mathrm{CD}|\cos\theta_2 \\ y_C = y_D - |\mathrm{CD}|\sin\theta_2 \end{cases} \tag{1.32}$$

Combining Eqs. (1.27) and (1.32) yields the equation of the straight line BC:

$$\mathrm{y} = k_1 x + (y_C - k_1 x_C) \tag{1.33}$$

Substituting Eq. (1.29) into Eq. (1.33) yields the abscissa of point E:

$$x_\mathrm{E} = \frac{\tan\theta_1 \cdot x_C + y_C}{\tan\theta' + \tan\theta_1} \tag{1.34}$$

The condition $|\mathrm{OE}| \geq |\mathrm{OF}|$ should be met when the log-spiral curve GI is above the interface BC, i.e.

$$|x_\mathrm{E}|\sqrt{1 + (\tan\theta')^2} \geq r_0 \exp\left[\left(\theta' - \theta_0\right)\tan\varphi_m\right] \tag{1.35}$$

Similarly, the condition $\left|\mathrm{OE}'\right| \geq \left|\mathrm{OF}'\right|$ should be met, i.e.,

$$|x_{\mathrm{E}'}|\sqrt{1 + (\tan\theta'')^2} \geq r_0 \exp\left[\left(\theta'' - \theta_0\right)\tan\varphi_m\right] \tag{1.36}$$

where θ'' is determined using the following:

$$\frac{\tan\varphi_m \sin\theta'' + \cos\theta''}{\tan\varphi_m \cos\theta'' - \sin\theta''} + \tan\theta_2 = 0(0 < \theta'' < \pi) \tag{1.37}$$

$$x_{\mathrm{E}'} = \frac{\tan\theta_2(r_h\cos\theta_h - l_1\cos\beta) + (r_h\sin\theta_h + l_1\sin\beta)}{\tan\theta'' + \tan\theta_2} \tag{1.38}$$

Determining the Safety Factor. For Mode 2, the actual safety factor and its corresponding failure mechanism can be determined by using a constrained nonlinear optimization method. The strength reduction factor **F** is regarded as an objective function in a minimization problem:

$$\min F(\theta_0, \theta_h, l_1) \tag{1.39}$$

The constraints in Eq. (1.39) can be divided into three cases.

(1) $\theta_0 < \theta' \le \theta'' < \theta_h$

This case is shown in Fig. 1.3 and is applicable in most cases. The corresponding constraints are

$$s.t.\begin{cases} 0 \le \theta_0 \le \frac{\pi}{2} \\ \theta_0 < \theta_h \le \pi \\ 0 \le l_1 \le \frac{H}{\sin\beta} \\ Eq.(35) \\ Eq.(36) \end{cases} \tag{1.40}$$

(2) $\theta'' \ge \theta_h \ge \theta'$ or $\theta'' \ge \theta' \ge \theta_h$.

This case is shown in Fig. 1.4 and is applicable to the case with higher slope angle β and smaller θ_2 (i.e., E′ and F′ may be located outside the slope). Thus, the corresponding constraints are

$$s.t.\begin{cases} 0 \le \theta_0 \le \frac{\pi}{2} \\ \theta_0 < \theta_h \le \pi \\ 0 \le l_1 \le \frac{H}{\sin\beta} \\ Eq.(35) \end{cases} \text{or} \begin{cases} 0 \le \theta_0 \le \frac{\pi}{2} \\ \theta_0 < \theta_h \le \pi \\ 0 \le l_1 \le \frac{H}{\sin\beta} \end{cases} \tag{1.41}$$

(3) $\theta'' \ge \theta_0 \ge \theta'$ or $\theta_0 \ge \theta'' \ge \theta'$.

This case is shown in Fig. 1.5 and is applicable to smaller β and larger θ_1 values (i.e., E and F may be located outside the slope). The corresponding constraints are

$$s.t.\begin{cases} 0 \le \theta_0 \le \frac{\pi}{2} \\ \theta_0 < \theta_h \le \pi \\ 0 \le l_1 \le \frac{H}{\sin\beta} \\ Eq.(36) \\ |AB| \ge |AG| \end{cases} \text{or} \begin{cases} 0 \le \theta_0 \le \frac{\pi}{2} \\ \theta_0 < \theta_h \le \pi \\ 0 \le l_1 \le \frac{H}{\sin\beta} \\ |AB| \ge |AG| \end{cases} \tag{1.42}$$

where

$$|\mathrm{AB}| = \frac{\sin(\beta - \theta_2)\sin(\theta_1 + \theta_3)}{\sin\beta\sin(\theta_2 + \theta_3)\sin(\theta_1 - \alpha)}H \tag{1.43}$$

$$|\mathrm{AG}| = r_0\left\langle \frac{\sin(\theta_h - \theta_0)}{\sin(\theta_h + \alpha)} - \frac{\sin(\theta_h + \beta)}{\sin(\theta_h + \alpha)\sin(\beta - \alpha)} \right. \\ \left. \{\sin(\theta_h + \alpha)\exp[(\theta_h - \theta_0)\tan\varphi_m] - \sin(\theta_0 + \alpha)\}\right\rangle \tag{1.44}$$

For a specific problem, the optimum solution to Eq. (1.39) in each of the three aforementioned cases can be obtained.

1.2.3 Failure in Mode 3

The local failure mode on the surface of the slope was assumed to occur on the log-spiral surface GI, as shown in Fig. 1.6. Similar to Mode 2, the work-energy balance equation is

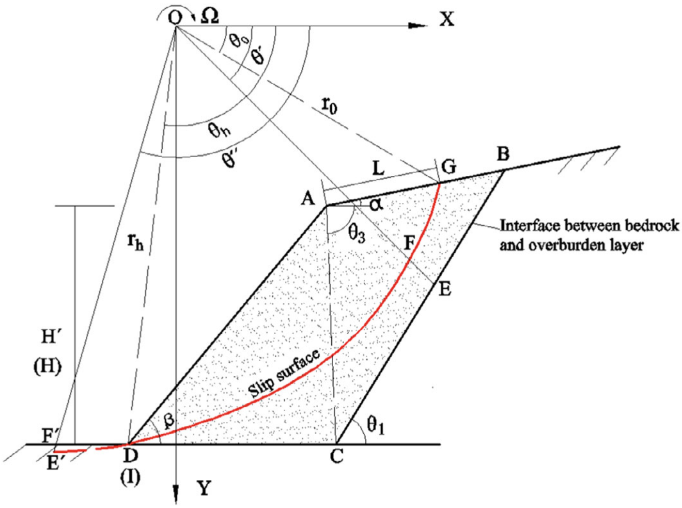

Fig. 1.4 Local failure of the slope with cracking at the top (case 2)

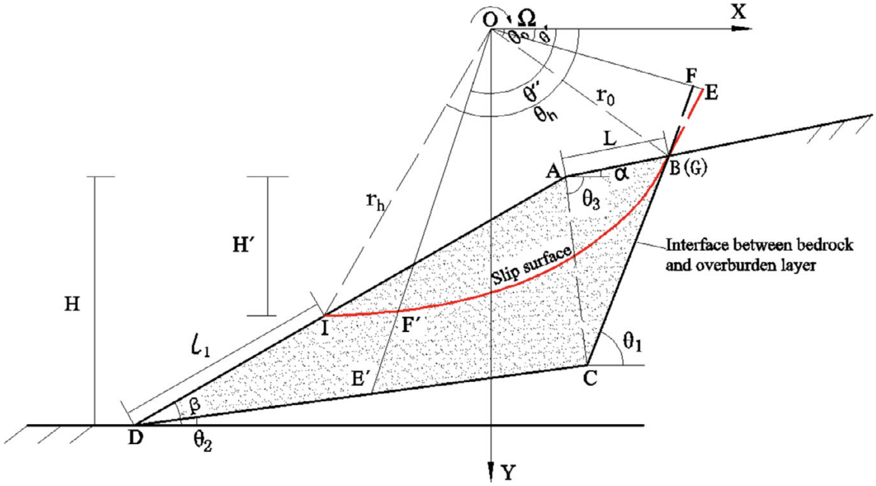

Fig. 1.5 Local failure of the slope with cracking at the top (case 3)

$$\gamma r_0(f_1 - f_4) = \frac{c_m}{2\tan\varphi_m}\{\exp[2(\theta_h - \theta_0)\tan\varphi_m] - 1\} \tag{1.45}$$

where f_1 is defined in Eq. (1.21).

$$f_4 = \frac{1}{6}\frac{H'}{r_0}\frac{\sin(\theta_h + \beta)}{\sin\beta}\exp[(\theta_h - \theta_0)\tan\varphi_m]\{\cos\theta_0 + \cos\theta_h\exp[(\theta_h - \theta_0)\tan\varphi_m]\} \tag{1.46}$$

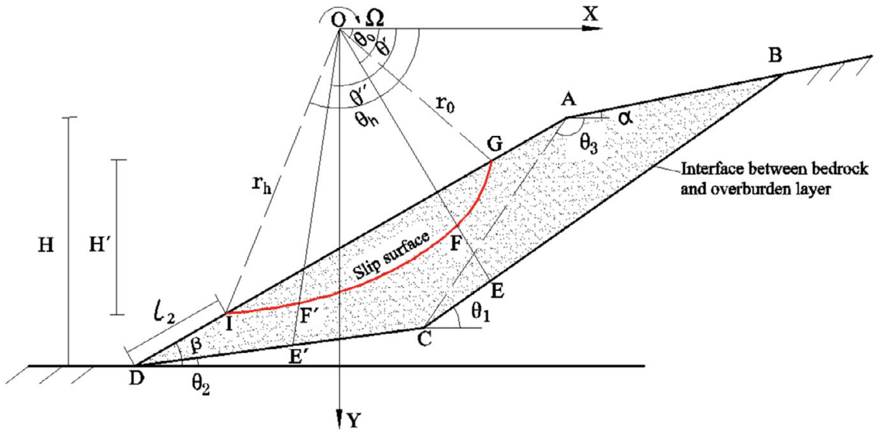

Fig. 1.6 Schematic showing local failure in Mode 3

$$r_0 = \frac{H'}{\{\sin\theta_h \exp[(\theta_h - \theta_0)\tan\varphi_m] - \sin\theta_0\}} \quad (1.47)$$

$$r_h = r_0 \exp[(\theta_h - \theta_0)\tan\varphi_m] \quad (1.48)$$

$$|x_{\mathrm{E}}|\sqrt{1 + (\tan\theta')^2} \geq r_0 \exp\left[\left(\theta' - \theta_0\right)\tan\varphi_m\right] \quad (1.49)$$

$$|x_{\mathrm{E}'}|\sqrt{1 + (\tan\theta')^2} \geq r_0 \exp\left[\left(\theta' - \theta_0\right)\tan\varphi_m\right] \quad (1.50)$$

The strength reduction factor F in Mode 3 is regarded as an objective function in a minimization problem:

$$\min F\left(\theta_0, \theta_h, l_2, H'\right) \quad (1.51)$$

where l_2 is the distance between the shear exit and the slope toe (i.e., DI). The constraints of Eq. (1.51) can be divided into the following three cases:

(1) $\theta_0 < \theta' \leq \theta' < \theta_h$

This case is shown in Fig. 1.6 and is applicable in most cases. The corresponding constraint is

$$s.t.\begin{cases} 0 \leq \theta_0 \leq \frac{\pi}{2} \\ \theta_0 < \theta_h \leq \pi \\ 0 \leq l_2 \leq \frac{H-H'}{\sin\beta} \\ 0 \leq H' \leq H \\ Eq.(49) \\ Eq.(50) \end{cases} \quad (1.52)$$

(2) $\theta' \geq \theta_h \geq \theta'$ or $\theta' \geq \theta' \geq \theta_h$.

This case is shown in Fig. 1.7 and is applicable to higher β and smaller θ_2 values (i.e., E′ and F′ may be located outside the slope). The corresponding constraint is

$$s.t.\begin{cases} 0 \leq \theta_0 \leq \frac{\pi}{2} \\ \theta_0 < \theta_h \leq \pi \\ 0 \leq l_2 \leq \frac{H-H'}{\sin\beta} \\ 0 \leq H' \leq H \\ Eq.(49) \end{cases} \text{or} \begin{cases} 0 \leq \theta_0 \leq \frac{\pi}{2} \\ \theta_0 < \theta_h \leq \pi \\ 0 \leq l_2 \leq \frac{H-H'}{\sin\beta} \\ 0 \leq H' \leq H \end{cases} \quad (1.53)$$

(3) $\theta' \geq \theta_0 \geq \theta'$ or $\theta_0 \geq \theta' \geq \theta'$.

This case is shown in Fig. 1.8 and is applicable to smaller β and larger θ_1 values (i.e., E and F may be located outside the slope). The corresponding constraint is